Supporting Information

Phosphorus Doping Induced Kinetics Modulation for Nitrogen Doped Carbon Mesoporous Nanotubes as Superior Alkali Metal Anode Beyond Lithium for High Energy Potassium-Ion Hybrid Capacitors

Jie Li,[a] Lai Yu,[a] Yapeng Li,[a] Gongrui Wang,[a] Liping Zhao,[a] Bo Peng,[a] Suyuan Zeng[b] Liang Shi*[a] and Genqiang Zhang*[a]

[a] Hefei National Laboratory for Physical Sciences at the Microscale, CAS Key Laboratory of Materials for Energy Conversion, Department of Materials Science and Engineering, University of Science and Technology of China, Hefei 230026, China

[b] Department of Chemistry and Chemical Engineering, Liaocheng University, Liaocheng 252059, China

*To whom the correspondence should be referred. Email:gqzhangmse@ustc.edu.cn; sliang@ustc.edu.cn

Experimental Section

Synthesis of PNC-MeNTs: In a typical process, 3 mmol of $MnSO_4 \cdot H_2O$, 2 mmol of $KMnO_4$ and 2 mmol NH_4F were orderly added into 40 mL of deionized water, respectively. The solution was transferred to a 50 mL Teflon-lined autoclave and kept at 150 ^oC for 12 h, then allowed to naturally cooled to room temperature. The product of MnO_2 was collected by centrifugation and washed with deionized water and ethanol. Subsequently, the pyrrole (0.38 mL) and aniline (0.29 mL) monomers were dissolved in 50 mL of H_2SO_4 solution (0.1 M) and phytic acid solution (PA, 0.5 M), in which the molar ratio of PA to pyrrole and aniline is 1:1. The MnO_2 nanowires (100 mg) were dispersed into deionized water by sonication 10 minutes and then added to the pyrrole/aniline/phytic acid (Py/AN/PA) solution under stirring for 4 h at room temperature. The obtained precipitate (denoted as PPy-PANI-PA) was washed with deionized water and ethanol several times and dried at 80 ^oC overnight. The black precursor was calcinated in a tubular furnace at 700 ^oC for 2 h with a ramp of 2 ^oC min^{-1} in Ar atmosphere to form the final product of P/N codoped carbon mesoporous nanotubes (denoted as PNC-MeNTs). Meanwhile, the precursor PPy-PANI-PA also calcinated at other temperatures (650 and 800 ^oC) under Ar atmosphere. Besides, the nitrogen-doped carbonaceous mesoporous nanotubes (denoted as NC-MeNTs) were synthesized with the similar method without the addition of PA.

Materials Characterization: The morphologies and microstructures of the synthesized materials were characterized by field-emission scanning electron microscopy (FESEM, JSM-6700F, Japan), transmission electron microscopy (TEM, JOEL, JEM-2010; Talos F200X). X-ray diffraction (XRD, TTR-III, Japan) and Raman spectrometer (Renishaw inVia) were used to collected analyze the structural

information of the obtained samples. The surface chemical state of the obtained samples was performed by X-ray photoelectron spectroscopy (XPS, ESCALAB 250). The specific surface area and pore distribution were investigated via Brunauer-Emmett-Teller (BET; Tristar II 3020M).

Electrochemical Measurement: LIR2016 coin-type cells were assembled for all electrochemical measurements. The SIBs and KIBs used pure sodium or potassium foil as the counter electrodes and assembled in an argon-filled glove, a glass microfiber filters (Whatman, GF/F) as the separator, 1.0 M $NaClO_4$ in EC: DEC=1:1 Vol% with 5.0% FEC and 1.0 M KFSI in EMC=100 Vol% as the electrolytes, respectively. The active materials, carbon black (Super-P) and polyvinylidene difluoride (PVDF) binder (the weight ratio 70:20:10) were mixed in N-methyl-2-pyrrolidinone (NMP) solvent. The slurry coated on copper foil and dried in a vacuum oven at 100 ºC for 12 h. The mass loadings of the anode materials are 0.8-1.0 mg cm^{-2}. Galvanostatic charge/discharge measurements were tested on a Neware BTS-610 battery tester. Cyclic voltammetry (CV) and electrochemical impedance spectroscopy (EIS) were measured by a CHI 660B electrochemical workstation.

Fabrication of Potassium ion Hybrid Capacitors: For the Potassium-ion hybrid capacitors (KIHCs), the PNC-MeNT//AC KIHCs devices were assembled employing the preactivated PNC-MeNT anode and active carbon (AC) cathode with a mass ratio ranging from 1:1 to 1:3. The AC electrode was constructed by mixing AC, Super-P and PVDF (the weight ratio 70:20:10) on aluminum foils. The PNC-MeNT anode in K-half cells was cycled for 5 cycles at 0.1 A g^{-1} and then assembled with AC cathode in the Ar-filled glove box. The energy/power density of the PNC-MeNT//AC KIHCs was calculated based on the following equations:[1]

$$E = P X t \qquad (1)$$

$$P = V_{ave} X i / m \quad (2)$$

$$V_{ave} = (V_{max} + V_{min}) / 2 \quad (3)$$

Where *t* is the discharge time, *i* is the discharge current, *m* is the total mass of the active materials in both anode and cathode, and V_{max} is the potential at the beginning of discharge after the *IR* drop, V_{min} is voltage at the end of the discharge.

1. Characterization

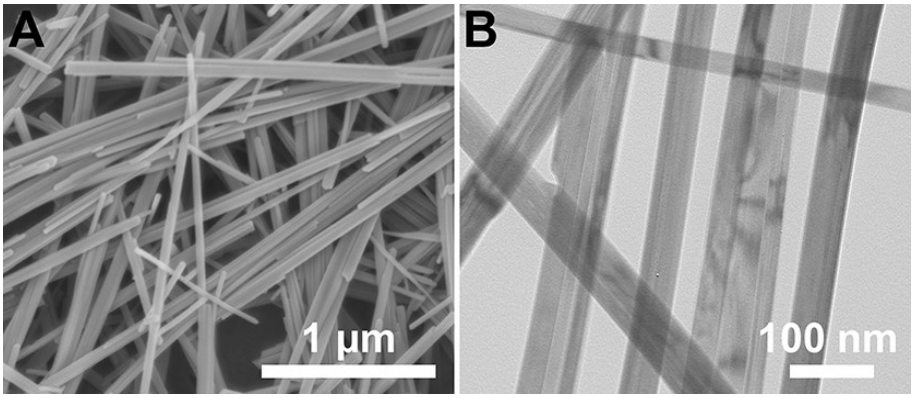

Figure S1. (A) The FESEM and (B) TEM images of the MnO_2 nanowires.

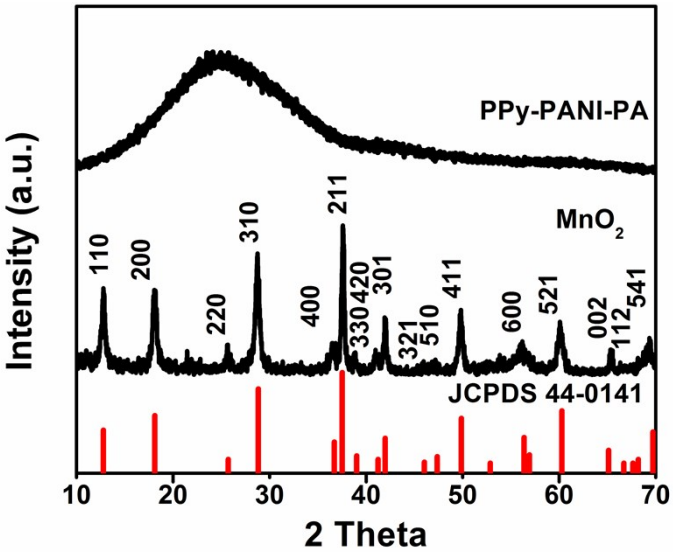

Figure S2. XRD patterns of MnO_2 nanowires and PPy-PANI-PA composite nanotubes.

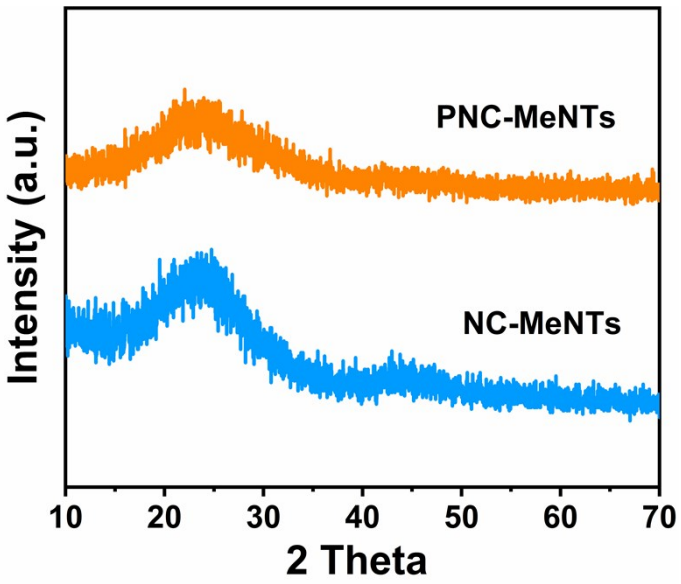

Figure S3. XRD patterns of PNC-MeNTs and NC-MeNTs.

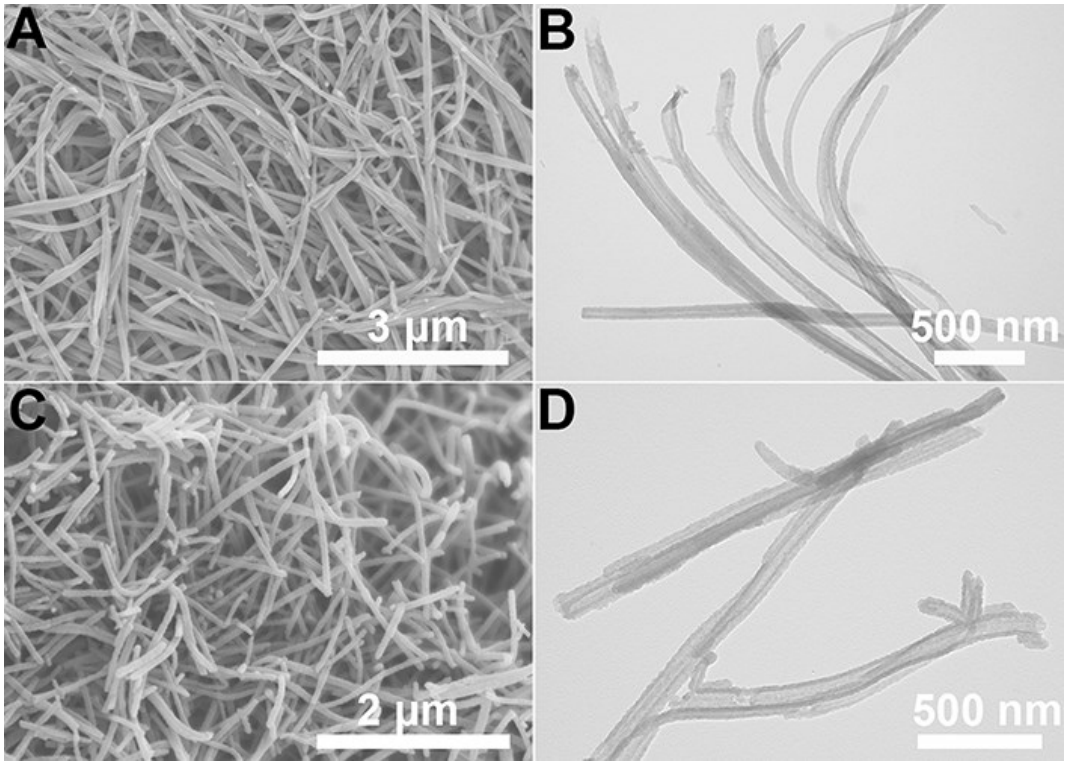

Figure S4. The SEM (A) and TEM (B) images of the NC-MeNTs precursor; the SEM (C) and (D) TEM images of the NC-MeNTs.

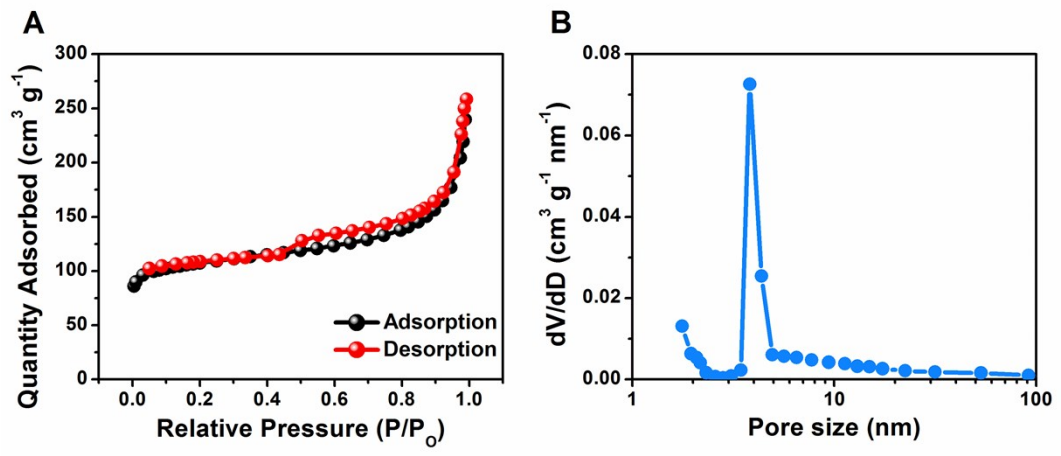

Figure S5. N_2 adsorption/desorption isotherm (A) and pore-size distribution (B) of NC-MeNTs.

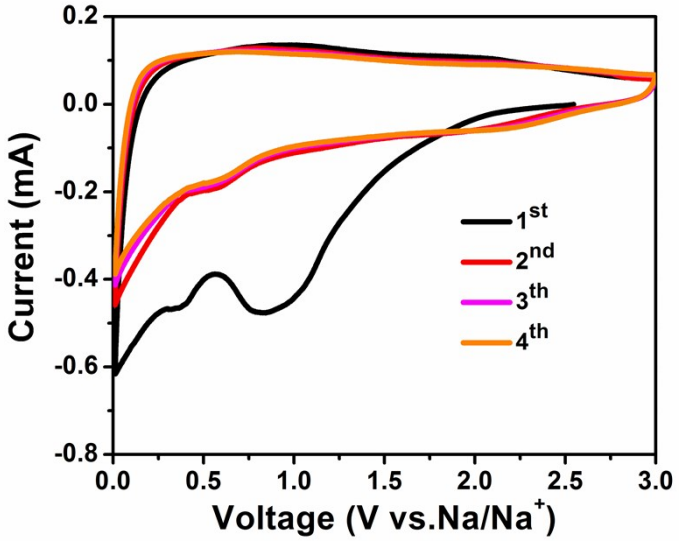

Figure S6. CV curves of PNC-MeNT anode at a scan rate of 0.2 mV s^{-1} for Na^+ storage.

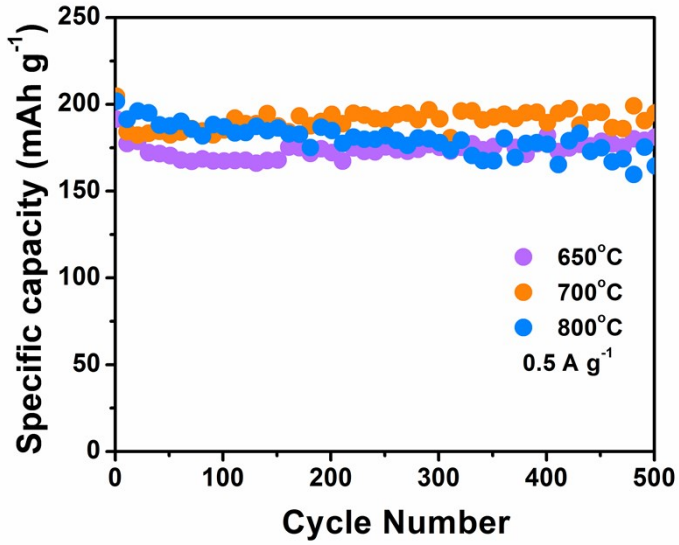

Figure S7. Cycling performance of PNC-MeNTs samples calcinated at different temperatures at a current density of 0.5 A g^{-1} for SIBs.

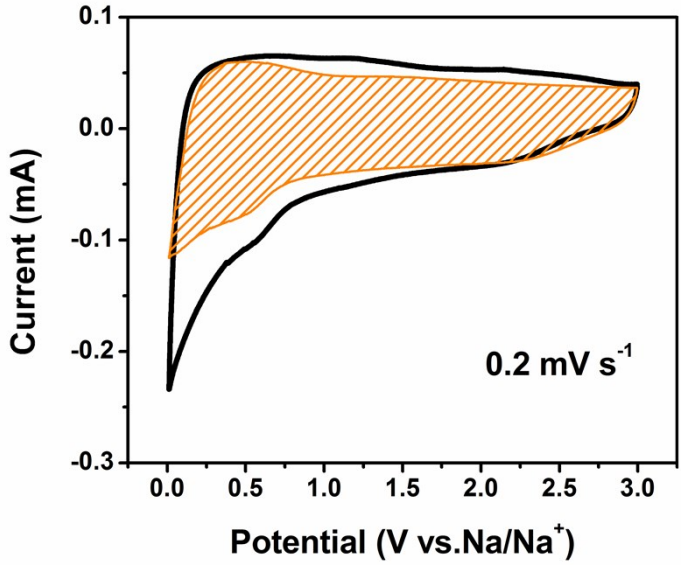

Figure S8. Capacitive contribution (shaded region) at a scan rate of 0.2 mV s^{-1} of PNC-MeNTs for SIBs.

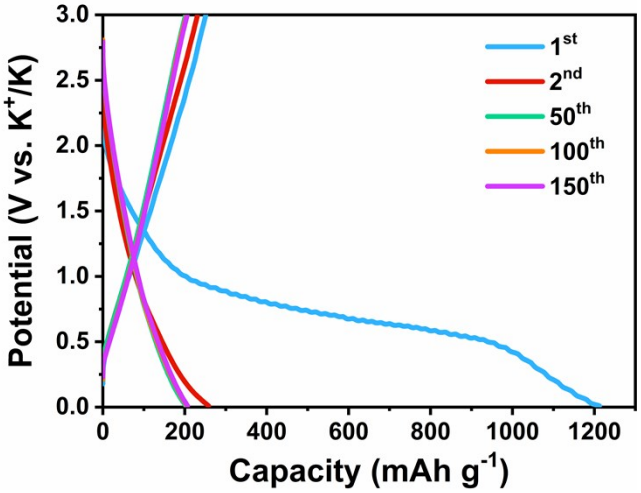

Figure S9. The charge/discharge profiles of PNC-MeNTs at 0.1 A g^{-1} for KIBs.

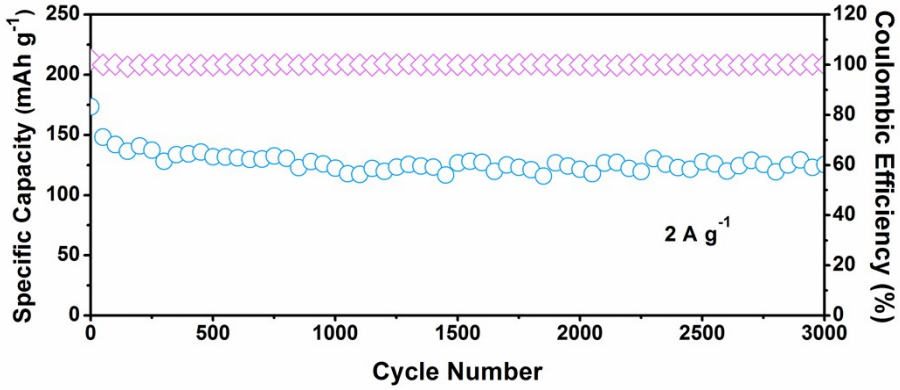

Figure S10. Long cycling performance of the PNC-MeNTs at a high current density of 2 A g^{-1} over 3000 cycles.

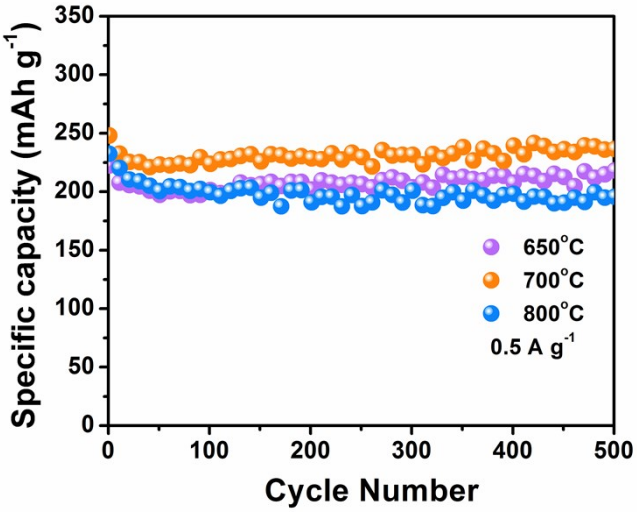

Figure S11. Cycling stability of PNC-MeNTs samples calcinated at different temperatures at 0.5 A g^{-1} for KIBs.

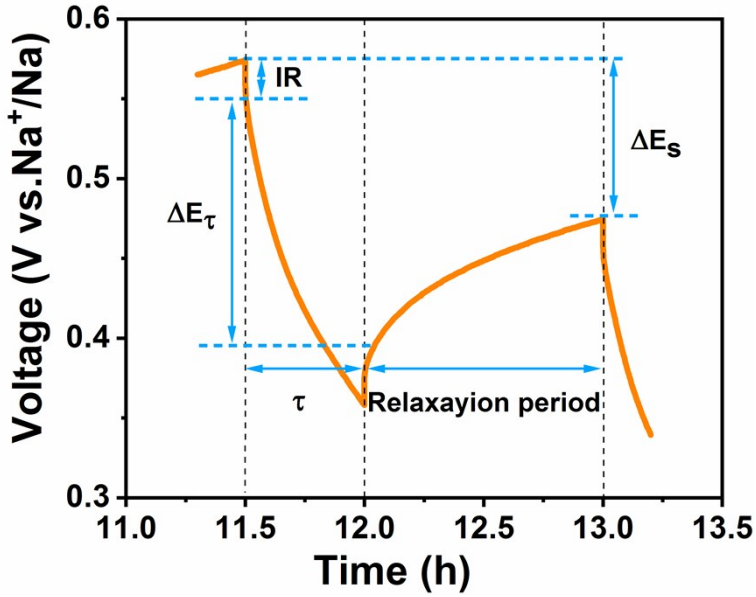

Figure S12. *ΔEs* and *ΔEτ* profile of PNC-MeNTs during discharge process for SIBs.

The galvanostatic intermittent titration (GITT) technique is employed to ascertain the effect on sodium/potassium ion diffusion kinetics with a pulse current at 0.05 A g^{-1} for 30 min between rest intervals for 60 min. The diffusion coefficient (D) can be calculated from the following equation: [2, 3]

$$D = \frac{4}{\pi\tau}\left(\frac{m_B V_M}{M_B S}\right)^2 \left(\frac{\Delta E_S}{\Delta E_\tau}\right)^2 \quad (4)$$

Where τ is the time duration of the current pulse; m_B is the mass loading of the active material; V_M is the molar volume of the electrode; M_B is the molar mass of electrode material; S is the area of the electrode; ΔEs is the steady-state voltage change between before and after the current pulse; $\Delta E\tau$ is the voltage change during the current pulse.

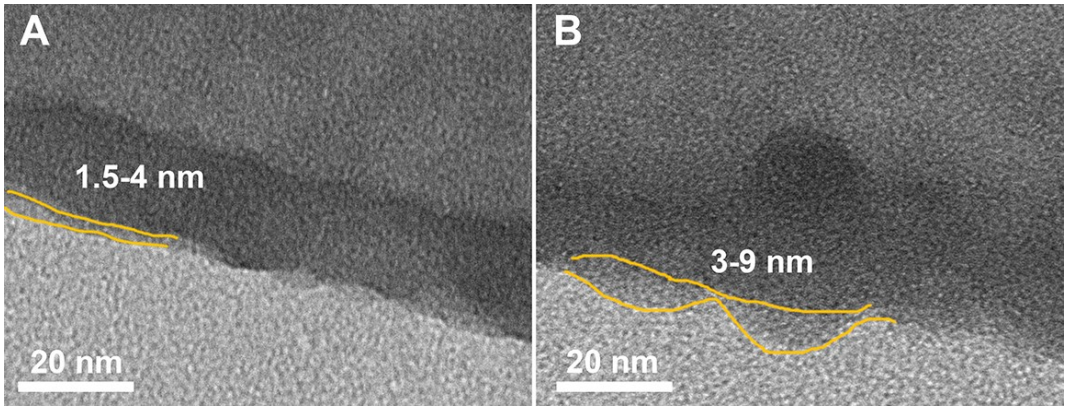

Figure S13. The TEM images of PNC-MeNTs after discharged to 0.01 V at 0.01 A g^{-1} in SIBs (A) and KIBs (B).

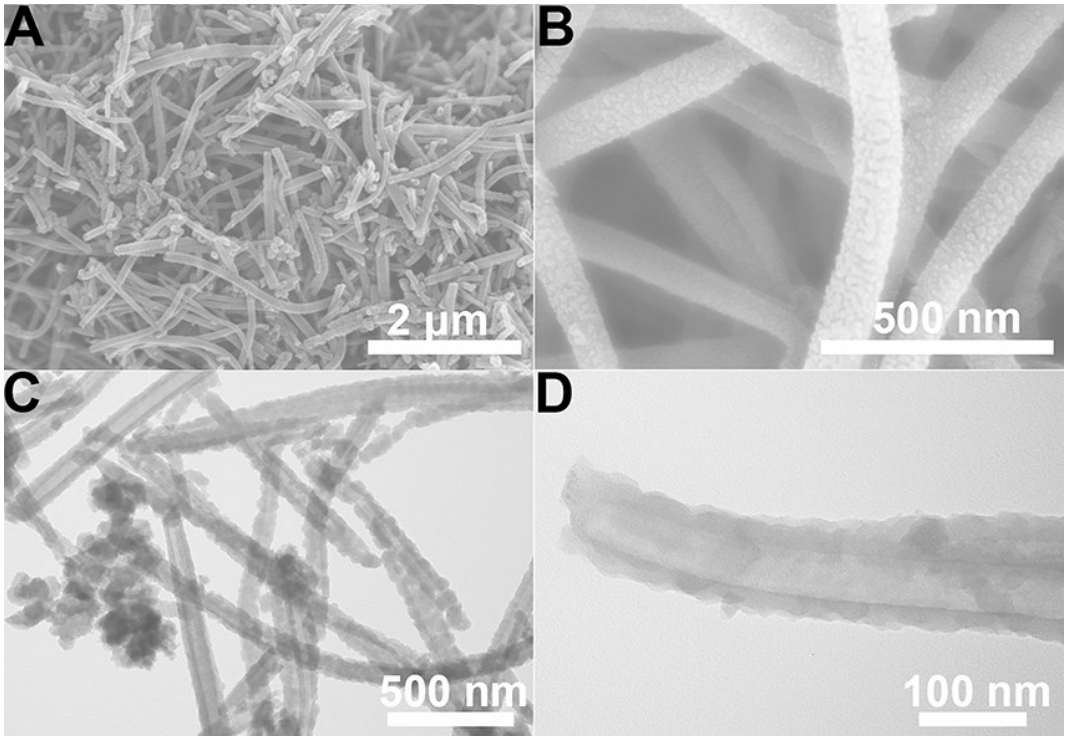

Figure S14. The SEM (A, B) and TEM (C, D) images of PNC-MeNTs after 200 cycles at 0.1 A g^{-1} for SIBs.

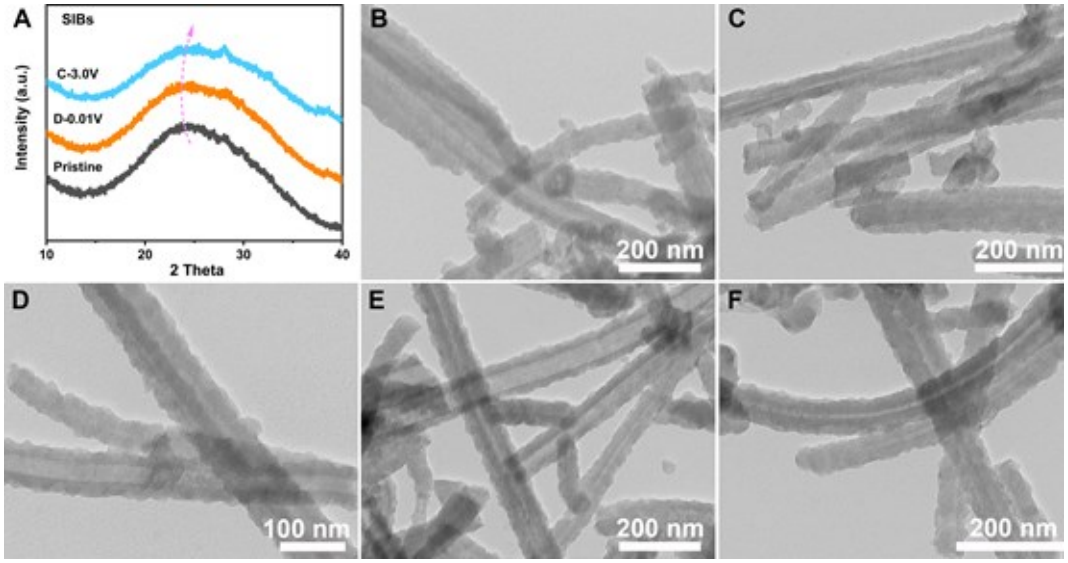

Figure S15. The ex situ XRD patterns (A); The TEM images of PNC-MeNTs in different sodiation/ desodiation states at a current density of 0.1 A g^{-1}: the initial state(B), discharged to 1.5 V (C) and 0.01 V (D), charged to 1.5 V (E) and 3.0 V (F).

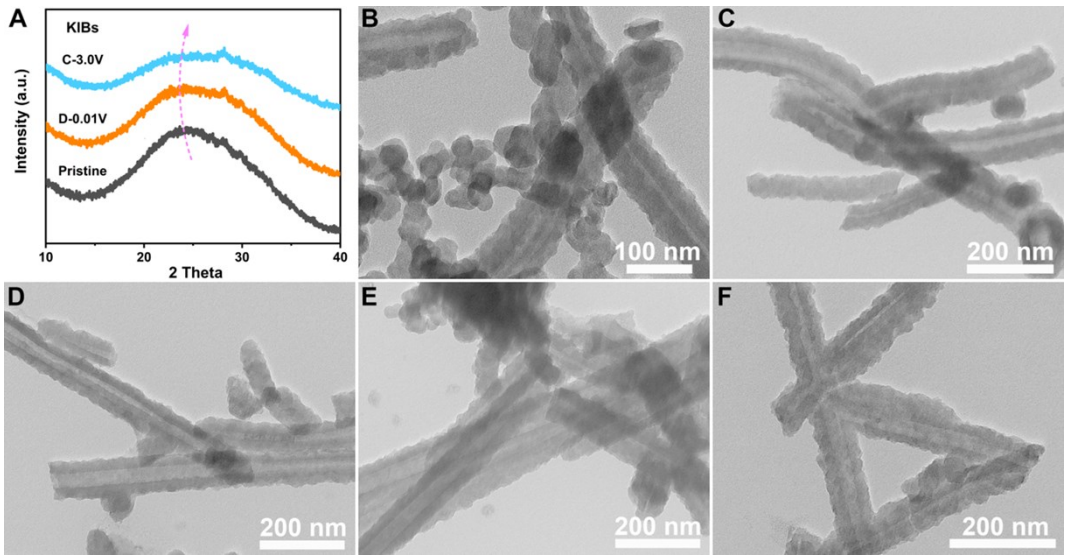

Figure S16. The ex situ XRD patterns (A); The TEM images of PNC-MeNTs in different potassiation/depotassiation states at a current density of 0.1 A g^{-1}: the initial state(B), discharged to 1.5 V (C) and 0.01 V (D), charged to 1.5 V (E) and 3.0 V (F).

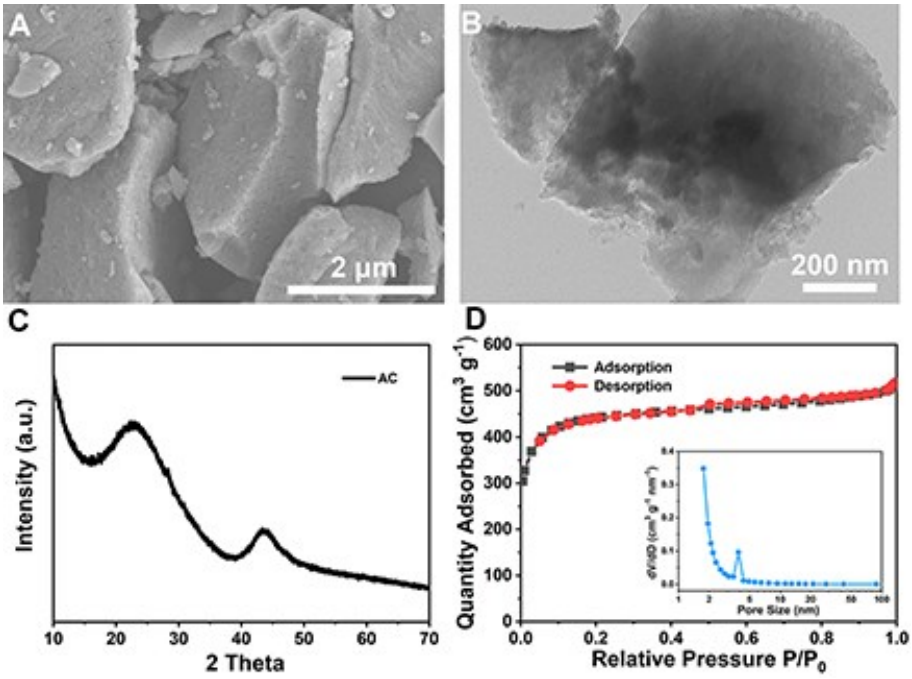

Figure S17. (A) The SEM; (B) TEM images; (C) XRD pattern and (D) N_2 adsorption/desorption isotherm (inset: pore-size distribution) for commercial AC.

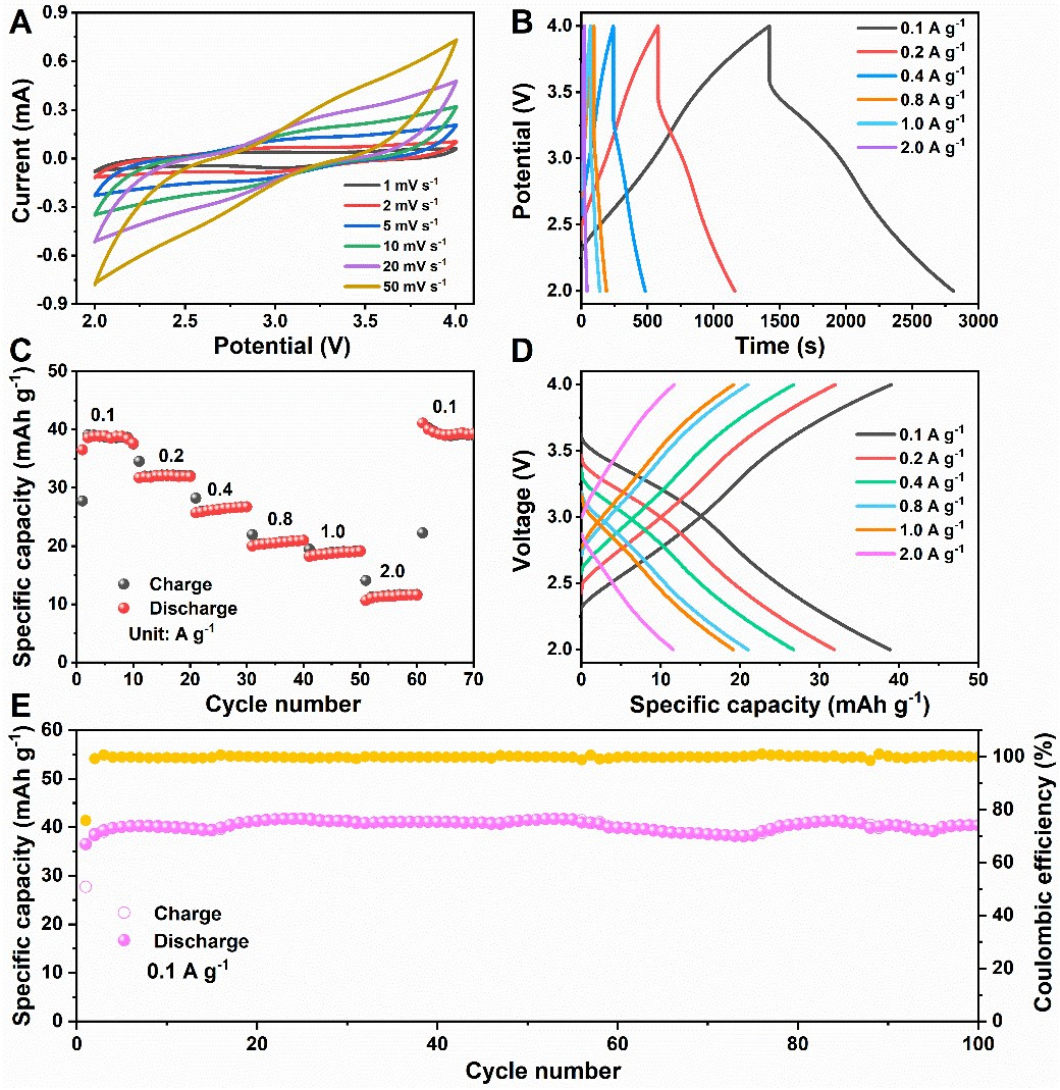

Figure S18. (A) CV curves at various scan rates and GCD curves at various current densities of AC electrode in 2.0-4.0 V (B); (C) Rate performance and (E) charge/discharge curves at different current densities of AC; (F) Cycling stability of AC at a current density of 0.1 A g^{-1} in half cell.

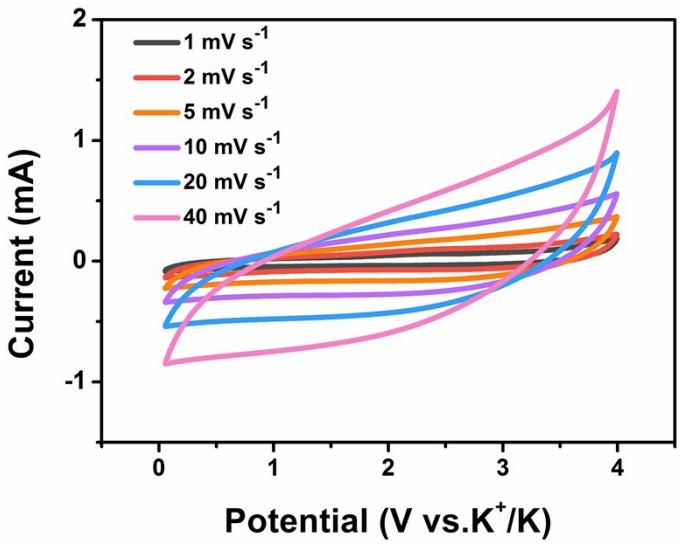

Figure S19. CV curves at different scan rates of the PNC-MeNT//AC KIHCs with the mass ratio of 1:1.5.

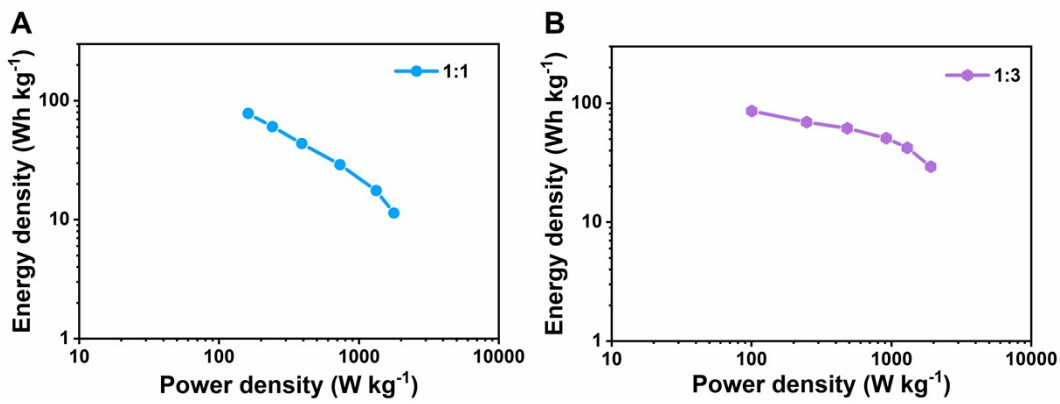

Figure S20. Ragone plot of the PNC-MeNT//AC KIHCs with mass ratios of 1:1 (A) and 1:3 (B).

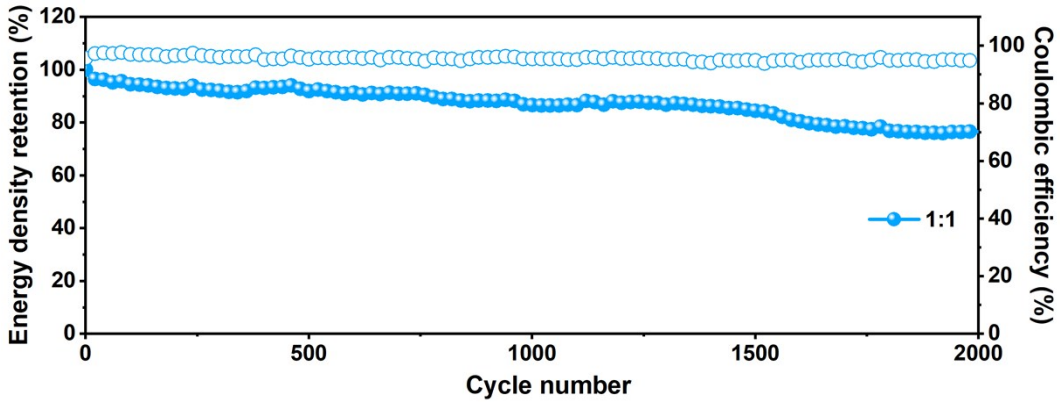

Figure S21. Cycling performance of the PNC-MeNT//AC KIHCs with the mass ratio of 1:1 at 0.8 A g^{-1}.

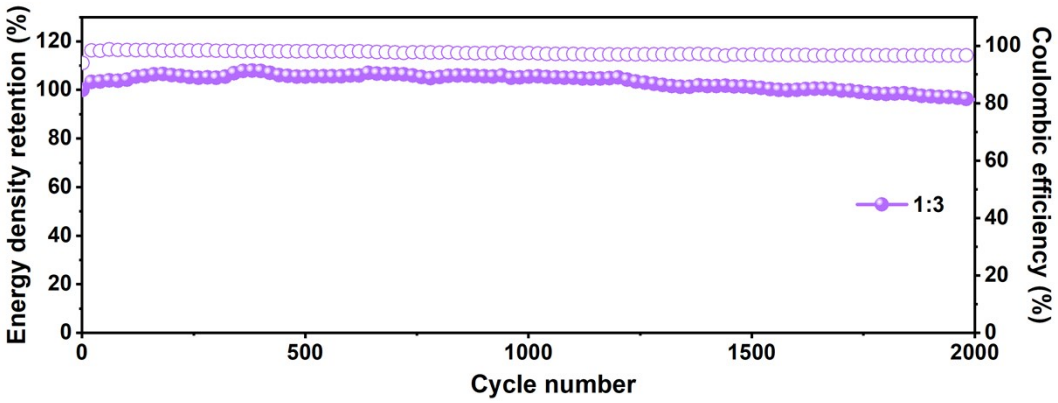

Figure S22. Cycling stability of the PNC-MeNT//AC KIHCs with the mass ratio of 1:3 at 0.8 A g^{-1}.

Table S1. Elemental analysis of PNC-MeNTs and NC-MeNTs.

Atomic content [%]	C	N	P
PNC-MeNTs	81.39	15.03	3.58
NC-MeNTs	87.52	12.48	---

Table S2. Comparison of the electrochemical performances of reported carbon-based carbon materials for SIBs.

Materials	Rate capability (mAh g^{-1})	Cyclability (mAh g^{-1})	Reference
P-CNSs	269 at 0.2 A g^{-1} 235 at 0.5 A g^{-1} 208 at 1 A g^{-1} 169 at 2 A g^{-1} 143 at 5 A g^{-1} 117 at 10 A g^{-1}	196.9/1000 cycle/1 A g^{-1} 108.8/5000 cycle/5 A g^{-1}	Ref 4
N, P-doped carbon sheets	233 at 0.1 A g^{-1} 204 at 0.2 A g^{-1} 177 at 0.5 A g^{-1} 143 at 1 A g^{-1} 122 at 2 A g^{-1}	202/200 cycle/0.2 A g^{-1} 103/2000 cycle/1 A g^{-1}	Ref 5
3D PCFs	290 at 0.2 A g^{-1} 253 at 0.5 A g^{-1} 200 at 1 A g^{-1} 166 at 2 A g^{-1} 130 at 5 A g^{-1} 104 at 10 A g^{-1}	99.8/10 000 cycle/5 A g^{-1}	Ref 6
SC-NS	232.2 at 0.02 A g^{-1} 103.8 at 1 A g^{-1}	128.7/3500 cycle/0.8 A g^{-1}	Ref 7
3DFC-700	278 at 0.1 A g^{-1} 227 at 0.2 A g^{-1} 199 at 0.5 A g^{-1}	175/1000 cycle/0.5 A g^{-1} 99/10 000 cycle/10 A g^{-1}	Ref 8

	176 at 2 A g-1 127 at 10 A g^{-1}		
huCP/g-C_3N_4	264 at 0.1 A g^{-1} 231 at 0.2 A g^{-1} 162 at 0.5 A g^{-1} 134 at 1 A g^{-1} 116 at 2 A g^{-1} 93 at 5 A g^{-1} 64 at 10 A g^{-1}	110/4000 cycle/1 A g^{-1}	Ref 9
PCS	317 at 0.1 A g^{-1} 204 at 0.2 A g^{-1} 151 at 0.5 A g^{-1} 116 at 1 A g^{-1} 91 at 2 A g^{-1} 70 at 5 A g^{-1}	240/200 cycle/0.1 A g^{-1}	Ref 10
FP-MP 5:2 1000	281 at 0.03 A g^{-1} 259 at 0.06 A g^{-1} 227 at 0.15 A g^{-1} 174 at 0.3 A g^{-1} 121 at 0.6 A g^{-1} 78 at 1.2 A g^{-1}	191/150 cycle/0.15 A g^{-1}	Ref 11
Carbon derived from sweet gum	339.1 at 0.05 A g^{-1} 281.7 at 0.1 A g^{-1} 237.4 at 0.2 A g^{-1} 169.6 at 0.5 A g^{-1} 138.3 at 1 A g^{-1}	136.1/1000 cycle/1 A g^{-1}	Ref 12
PNC-MeNTs	**283.5 at 0.1 A g^{-1}** **239.0 at 0.2 A g^{-1}** **216.2 at 0.5 A g^{-1}** **192.5 at 1 A g^{-1}** **174.1 at 2 A g^{-1}**	**256.2/200 cycle/0.1 A g^{-1}** **214.1/1000 cycle/1 A g^{-1}** **94.7/10 000 cycle/10 A g^{-1}**	**This work**

	147.3 at 5 A g^{-1} **123.3 at 10 A g^{-1}**		

Table S3. Comparison of the electrochemical performances of reported carbon-based carbon materials for KIBs.

Materials	Rate capability (mAh g^{-1})	Cyclability (mAh g^{-1})	Reference
OMC	286.1 at 0.05 A g^{-1} 255.1 at 0.1 A g^{-1} 218.8 at 0.2 A g^{-1} 186.3 at 0.5 A g^{-1} 144.2 at 1 A g^{-1}	146.5/1000 cycle/1 A g^{-1}	Ref 13
S/N@C	320 at 0.05 A g^{-1} 235 at 0.1 A g^{-1} 160.2 at 0.5 A g^{-1} 123.5 at 1 A g^{-1} 91.2 at 2 A g^{-1}	200/400 cycle/0.1 A g^{-1} 65/900 cycle/1 A g^{-1}	Ref 14
PNCM	388 at 0.05 A g^{-1} 319 at 0.1 A g^{-1} 286 at 0.2 A g^{-1} 253 at 0.5 A g^{-1} 225 at 1 A g^{-1} 199 at 2 A g^{-1}	152/3000 cycle/1 A g^{-1}	Ref 15
SC-NS	247 at 0.1 A g^{-1} 185 at 0.2 A g^{-1} 162 at 0.5 A g^{-1} 146 at 1 A g^{-1} 130 at 2 A g^{-1}	117.2/3000 cycle/1 A g^{-1}	Ref 16
3DFC-700	340 at 28 mA g^{-1} 301 at 56 mA g^{-1}	250/150 cycle/0.14 A g^{-1} ~153/500 cycle/0.28 A g^{-1}	Ref 17

	253 at 140 mA g^{-1} 204 at 280 mA g^{-1} 117 at 560 mA g^{-1}		
MCOs	354 at 0.05 A g^{-1} 317 at 0.1 A g^{-1} 223 at 0.2 A g^{-1} 178 at 0.5 A g^{-1} 110 at 1 A g^{-1}	100/1300 cycle/1 A g^{-1} 80/3000 cycle/2 A g^{-1}	Ref 18
OLC	245 at 0.05 A g^{-1} 194 at 0.1 A g^{-1} 167 at 0.2 A g^{-1} 140 at 0.5 A g^{-1} 121 at 1 A g^{-1} 106 at 2 A g^{-1}	151/1000 cycle/0.5 A g^{-1} 111/1000 cycle/2 A g^{-1}	Ref 19
N-HCNs	326 at 0.05 A g^{-1} 252 at 0.1 A g^{-1} 210 at 0.2 A g^{-1} 182 at 0.5 A g^{-1} 162 at 1 A g^{-1} 141 at 2 A g^{-1}	201/100 cycle/0.1 A g^{-1} 154/2500 cycle/1 A g^{-1}	Ref 20
NOGCN	476 at 0.05 A g^{-1} 114 at 1 A g^{-1}	131/300 cycle/0.5 A g^{-1}	Ref 21
PNC-MeNTs	**258.6 at 0.1 A g^{-1}** **206.6 at 0.2 A g^{-1}** **169.6 at 0.5 A g^{-1}** **146.1 at 1 A g^{-1}** **106.9 at 2 A g^{-1}**	**210.2/150 cycle/0.1 A g^{-1}** **188.7/3000 cycle/1 A g^{-1}** **125.5/3000 cycle/2 A g^{-1}**	**This work**

Table S4. Comparison of the electrochemical performances of the PNC-MeNT//AC KIHCs with recent literatures about potassium ion hybrid capacitors.

Materials	Voltage window (V)	Energy density (Wh kg^{-1}) /Power density (W kg^{-1})	Cycling life	Reference
NHCS//ANHCS PIHC	0.01-4.0	114.2/100.5 19.1/8203	93%/2000/0.5 A g^{-1} 80.4%/5000/2 A g^{-1}	Ref 22
CTP@C//AC KIC	1.0-4.0	80/32 34/5144	75.9%/4000/5 A g^{-1}	Ref 23
PB//AC KIC	0-1.9	28/214 10.5/1890	98%/1200/2 A g^{-1}	Ref 24
KTO//NGC KIC	0-3.5	58.2/160 11.8/7200	75.5%/5000/1 A g^{-1}	Ref 25
graphite//AC KIC	0.5–3.5	12/22 11/1500	97%/55000	Ref 26
Co_2P@rGO//AC KIC	1.0-4.0	87/12 10/4264.7	68%/1000/1 A g^{-1}	Ref 27
$FeSe_2$/AC PIHC	0.1-3.8	230/198 30/920	/	Ref 28
CFMS//CFMS PDIC	0.01-3.8	58/1158.2 39/7800	90%/10 000/2 A g^{-1}	Ref 29
NCNTs//AC KIHC	0.01-4	117.1/112.8 25.7/1713.4	81.6%/2000/1 A g^{-1}	Ref 30
SC//AC KIHC	0-4	120/96 13.3/599	97.5%/1500/0.75 A g^{-1}	Ref 31
N,P-doped C//ADPC	1-4.2	72/257	75.6%/2000/1 A g^{-1}	Ref 32

KIHC		18.5/5220		
NPG//AC KIHC	1-4	104.4/760.6 41.6/14976	~65%/1000/1 A g^{-1}	Ref 33
HC//AC KIHC	1.5-4.2	77/2830 4.5/5000	84%/50/0.4 A g^{-1}	Ref 34
S-N-PCNs//AC KIHC	0.01-4.0	187/99 76/5136	86.4%/3000/1 A g^{-1}	Ref 35
PNC-MeNT//AC KIHC	**0.05-4.0**	**175.1@160.6 31.6@3034**	**85.8%/3000/0.8 A g^{-1}**	**This work**

Reference:

1. J. Chen, B. Yang, H. Hou, H. Li, L. Liu, L. Zhang and X. Yan, *Adv. Energy Mater.*, 2019, **9**, 1803894.
2. H. He, D. Huang, Y. Tang, Q. Wang, X. Ji, H. Wang and Z. Guo, *Nano Energy*, 2019, **57**, 728-736.
3. Y. Wang, D. Zhang, Y. Wang, Y. Zhang, X. Liu, W. Zhou, J.-K. Kim and Y. Luo, *Nanoscale*, 2019, **11**, 11025-11032.
4. H. Hou, L. Shao, Y. Zhang, G. Zou, J. Chen and X. Ji, *Adv. Sci.*, 2017, **4**, 1600243.
5. D. Qin, Z. Liu, Y. Zhao, G. Xu, F. Zhang and X. Zhang, *Carbon*, 2018, **130**, 664-671.
6. H. Hou, C. E. Banks, M. Jing, Y. Zhang and X. Ji, *Adv. Mater.*, 2015, **27**, 7861-7866.
7. X. Yao, Y. Ke, W. Ren, X. Wang, F. Xiong, W. Yang, M. Qin, Q. Li and L. Mai, *Adv. Energy Mater.*, 2018, **9**, 1803260.
8. B. Yang, J. Chen, S. Lei, R. Guo, H. Li, S. Shi and X. Yan, *Adv. Energy Mater.*, 2018, **8**, 1702409.
9. H. Tao, L. Xiong, S. Du, Y. Zhang, X. Yang and L. Zhang, *Carbon*, 2017, **122**, 54-63.
10. F. Sun, K. Wang, L. Wang, T. Pei, J. Gao, G. Zhao and Y. Lu, *Carbon*, 2019, **155**, 166-175.
11. F. Xie, Z. Xu, A. C. S. Jensen, H. Au, Y. Lu, V. Araullo-Peters, A. J. Drew, Y. S. Hu and M. M. Titirici, *Adv. Funct. Mater.*, 2019, **29**, 1901072.
12. K. Wang, Y. Xu, Y. Li, V. Dravid, J. Wu and Y. Huang, *J. Mater. Chem. A*, 2019, **7**, 3327-3335.
13. W. Wang, J. Zhou, Z. Wang, L. Zhao, P. Li, Y. Yang, C. Yang, H. Huang and S. Guo, *Adv. Energy Mater.*, 2018, **8**, 1701648.
14. A. Mahmood, S. Li, Z. Ali, H. Tabassum, B. Zhu, Z. Liang, W. Meng, W. Aftab, W. Guo, H. Zhang, M. Yousaf, S. Gao, R. Zou and Y. Zhao, *Adv. Mater.*, 2019, **31**, 1805430.
15. Y. Xie, Y. Chen, L. Liu, P. Tao, M. Fan, N. Xu, X. Shen and C. Yan, *Adv. Mater.*, 2017, **29**, 1702268.
16. J. Qin, H. M. Kheimeh Sari, C. He and X. Li, *J. Mater. Chem. A*, 2019, **7**, 3673-3681.
17. D. S. Bin, X. J. Lin, Y. G. Sun, Y. S. Xu, K. Zhang, A. M. Cao and L. J. Wan, *J. Am. Chem. Soc.*, 2018, **140**, 7127-7134.
18. G. Xia, C. Wang, P. Jiang, J. Lu, J. Diao and Q. Chen, *J. Mater. Chem. A*, 2019, **7**, 12317-12324.
19. J. Chen, B. Yang, H. Li, P. Ma, J. Lang and X. Yan, *J. Mater. Chem. A*, 2019, **7**, 9247-9252.
20. J. Ruan, X. Wu, Y. Wang, S. Zheng, D. Sun, Y. Song and M. Chen, *J. Mater. Chem. A*, 2019, **7**, 19305-19315.

21. Y. Sun, D. Zhu, Z. Liang, Y. Zhao, W. Tian, X. Ren, J. Wang, X. Li, Y. Gao, W. Wen, Y. Huang, X. Li and R. Tai, *Carbon*, 2020, **167**, 685-695.
22. D. Qiu, J. Guan, M. Li, C. Kang, J. Wei, Y. Li, Z. Xie, F. Wang and R. Yang, *Adv. Funct. Mater.*, 2019, **29**, 1903496.
23. Z. Zhang, M. Li, Y. Gao, Z. Wei, M. Zhang, C. Wang, Y. Zeng, B. Zou, G. Chen and F. Du, *Adv. Funct. Mater.*, 2018, **28**, 1802684.
24. L. Zhou, M. Zhang, Y. Wang, Y. Zhu, L. Fu, X. Liu, Y. Wu and W. Huang, *Electrochim. Acta*, 2017, **232**, 106-113.
25. S. Dong, Z. Li, Z. Xing, X. Wu, X. Ji and X. Zhang, *ACS Appl. Mater. Interfaces*, 2018, **10**, 15542-15547.
26. A. Le Comte, Y. Reynier, C. Vincens, C. Leys and P. Azaïs, *J. Power Sources*, 2017, **363**, 34-43.
27. Y. Wang, Z. Zhang, G. Wang, X. Yang, Y. Sui, F. Du and B. Zou, *Nanoscale Horiz.*, 2019, **4**, 1394-1401.
28. J. Ge, B. Wang, J. Wang, Q. Zhang and B. Lu, *Adv. Energy Mater.*, 2019, **9**, 1903277.
29. Y. Feng, S. Chen, J. Wang and B. Lu, *J. Energy Chem.*, 2020, **43**, 129-138.
30. X. Li, M. Chen, L. Wang, H. Xu, J. Zhong, M. Zhang, Y. Wang, Q. Zhang, L. Mei, T. Wang, J. Zhu, B. Lu and X. Duan, *Nanoscale Horiz.*, 2020, DOI: 10.1039/d0nh00451k.
31. L. Fan, K. Lin, J. Wang, R. Ma and B. Lu, *Adv. Mater.*, 2018, **30**, 1800804.
32. X. Yu, M. Shao, X. Yang, C. Li, T. Li, D. Li, R. Wang and L. Yin, *Chin. Chem. Lett.*, 2020, **31**, 2215-2218.
33. Y. Luan, R. Hu, Y. Fang, K. Zhu, K. Cheng, J. Yan, K. Ye, G. Wang and D. Cao, *Nano-Micro Lett.*, 2019, **11**, 30.
34. F. Wang, X. Wang, Z. Chang, X. Wu, X. Liu, L. Fu, Y. Zhu, Y. Wu and W. Huang, *Adv. Mater.*, 2015, **27**, 6962-6968.
35. X. Hu, Y. Liu, J. Chen, L. Yi, H. Zhan and Z. Wen, *Adv. Energy Mater.*, 2019, **9**, 1901533.